# Coarsening of sand ripples in mass transfer models

E. K. O. Hellén*
*Laboratory of Physics, Helsinki University of Technology, P.O. Box 1100, FIN-02150 HUT, Finland*

J. Krug†
*Fachbereich Physik, Universität Essen, 45117 Essen, Germany*

(Received 5 March 2002; published 23 July 2002)

Coarsening of sand ripples is studied in a one-dimensional stochastic model, where neighboring ripples exchange mass with algebraic rates, $\Gamma(m)\sim m^{\gamma}$, and ripples of zero mass are removed from the system. For $\gamma<0$, ripples vanish through rare fluctuations and the average ripple mass grows as $\langle m\rangle(t)\sim -\gamma^{-1}\ln(t)$. Temporal correlations decay as $t^{-1/2}$ or $t^{-2/3}$ depending on the symmetry of the mass transfer, and asymptotically the system is characterized by a product measure. The stationary ripple mass distribution is obtained exactly. For $\gamma>0$, ripple evolution is linearly unstable, and the noise in the dynamics is irrelevant. For $\gamma=1$, the problem is solved on the mean-field level, but the mean-field theory does not adequately describe the full behavior of the coarsening. In particular, it fails to account for the numerically observed universality with respect to the initial ripple size distribution. The results are not restricted to sand ripple evolution since the model can be mapped to zero range processes, urn models, exclusion processes, and cluster-cluster aggregation.

DOI: 10.1103/PhysRevE.66.011304 PACS number(s): 45.70.−n, 47.54.+r, 05.45.−a, 05.10.−a

## I. INTRODUCTION AND MOTIVATION

When a surface of sand is exposed to wind or water flow, patterns such as ripples or dunes are commonly formed. The physics of this process is extremely complex because it involves the interaction of a granular medium with a possibly turbulent hydrodynamic flow [1]. It is therefore desirable to develop simplified models that capture some of the key features of the pattern formation.

In this paper we are concerned with a class of models which focus on the role of the mass transfer in the evolution of the pattern. Along a one-dimensional cut perpendicular to the ripples, the pattern is described by a set $\{\lambda_i\}$ of ripple lengths, where the index $i$ labels the ripples in the array. The $\lambda_i$ are used here as a general measure of ripple size, without reference to the detailed geometry of individual ripples (see Fig. 1). In particular, we do not distinguish between the linear size of a ripple and the mass it contains (for further discussion of this point see [3]).

During the evolution of the patterns, the flow transfers mass between neighboring ripples. The central assumption of the model is that the mass transferred to ripple $i$ from ripple $i+1$ or $i-1$ (per unit time) is a function $\Gamma(\lambda_i)$ of the size of the ripple which gains the mass. Further motivation for this assumption will be given below. We refer to $\Gamma(\lambda)$ as the *robber function*.[1]

Depending on the characteristics of the flow, the mass transfer between ripples can be symmetric or asymmetric. In the symmetric case the balance between loss and gain processes for a given ripple leads to the evolution equation [3]

$$\frac{d\lambda_i}{dt}=\frac{1}{2}[-\Gamma(\lambda_{i-1})+2\Gamma(\lambda_i)-\Gamma(\lambda_{i+1})], \tag{1}$$

while in the asymmetric case (assuming, say, mass transfer only to the left) one has

$$\frac{d\lambda_i}{dt}=-\Gamma(\lambda_{i-1})+\Gamma(\lambda_i). \tag{2}$$

The factor 1/2 in Eq. (1) makes the time scales for both the dynamics equal.

A homogeneous state of equally sized ripples, $\lambda_i\equiv\overline{\lambda}$, is stationary under Eqs. (1) and (2), but its stability depends on the derivative of the robber function: The pattern is stable for $\Gamma'(\overline{\lambda})<0$ and unstable for $\Gamma'(\overline{\lambda})>0$ [3]. In the unstable case the dominant mode is a modulation of period 2, in which every second ripple grows and every second one shrinks. As the size of the shrinking ripples reaches zero in a finite time, the evolution equations (1) and (2) have to be supplemented by an *extinction rule*: When the size of a ripple vanishes, it is removed from the system and the remaining ripples are relabeled such that the previous neighbors of the removed ripple become neighbors of each other. Extinction events contribute to the *coarsening* of the pattern, i.e., to an increase of the mean wavelength. In this work the reverse process of ripple creation is not considered, hence coarsening is irreversible.

The symmetric mass transfer model (1) was first proposed as a description of vortex ripples in coastal waters, which are created under the oscillatory flow of surface waves [3]. In that context the dependence of the robber function on the size of the gaining ripple is motivated by the observation that the mass transfer is effectuated mostly by a separation vortex that appears in the wake of that ripple. Numerical simulations [3] and experiments [2] show that $\Gamma(\lambda)$ is nonmono-

*Electronic address: ehe@fyslab.hut.fi
†Electronic address: jkrug@Theo-Phys.Uni-Essen.DE

[1]This term was suggested to us by Ko van der Weele.

 

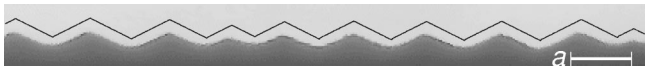


FIG. 1. Experimental image of vortex ripples in a one-dimensional annular geometry, published in [2]. The amplitude of the fluid oscillations is denoted by $a$. The line above the pattern shows a fit of triangles with a constant slope. Courtesy of K. H. Andersen.

tonic, with a maximum near $\lambda = a$, where $a$ is the amplitude of the fluid oscillations. Thus patterns of wavelength $\lambda < a (\lambda > a)$ are unstable (stable), and the main interest is in the wavelength selection process starting from a short wavelength, unstable state [2–4].

A related, asymmetric mass transfer model for wind driven sand ripples was introduced in [5]. The basic hypothesis of the model is that wind ripples wander with a speed that is inversely proportional to their size. This implies that a leading ripple (ripple $i+1$) is eroded by the trailing ripple (ripple $i$) at a rate which is proportional to $1/\lambda_i$, so the resulting evolution equation is of the type (2) with $\Gamma(\lambda) \sim 1/\lambda$. Since $\Gamma'(\lambda) < 0$, the homogeneous pattern is stable. However, when fluctuations are included by discretizing the ripple sizes and implementing a stochastic mass transfer rule, a fluctuation-driven coarsening mechanism becomes effective and leads to an increase of the mean wavelength with time $t$ as $\ln t$.

In this paper we consider a class of stochastic models whose noiseless counterparts are described by (1) or (2). We concentrate on monotonic, algebraic robber functions $\Gamma(\lambda) \sim \lambda^{\gamma}$ and study the coarsening process regarding $\gamma$ as a variable parameter. For $\gamma < 0$ this extends the results of [5] on fluctuation-driven coarsening. The case $\gamma > 0$ is a simple realization of linearly unstable ripple evolution, and it is studied here as a first step towards a better understanding of models with nonmonotonic robber functions [2–4]. Although the models are defined using the terminology of sand ripples, they are connected to other problems in nonequilibrium statistical physics. For example, for $\gamma = 0$ the system maps to coalescing random walks and is therefore exactly solvable. Other equivalences include exclusion processes, zero-range processes, urn models, and cluster-cluster aggregation.

Our main results are the following. In general, one can identify two time scales in the dynamics: The one of ripple extinctions and the other at which the system would equilibrate to a steady state in the absence of extinctions. For $\gamma < 0$ the loss of a ripple is a rare fluctuation when the mean ripple size is large. Therefore the two time scales are well separated, and the system has time to relax to a quasisteady state between ripple extinctions. We show that this state is characterized by a product measure. This justifies the mean-field assumption made in [5], and allows us to calculate the stationary ripple size distribution. The product measure becomes exact only at the limit $t \to \infty$ as the correlations in the system decay as a power law. The average ripple size grows logarithmically at late times, with a prefactor $-\gamma^{-1}$.

For $\gamma > 0$, extinctions are frequent events which occur on the same time scale as the evolution of the surviving ripples. We find in this case that the noise is irrelevant, so that the dynamics can be described by Eqs. (1) and (2). For $0 < \gamma < 1$ the mean ripple size grows algebraically with the exponent $1/(1-\gamma)$, while the growth is exponential for $\gamma = 1$. In the latter case the evolution equations become linear, and the problem can be solved exactly on the mean-field level. The mean-field theory reproduces the exponential growth for the mean ripple size, but incorrectly predicts a dependence of the ripple size distribution and the coarsening law on the initial conditions.

In the following section the model is introduced and its relations to other models are discussed. Algebraically decaying robber functions ($\gamma < 0$) are considered in Sec. III. The product form of the mass distribution is derived in Sec. III A, the coarsening law is calculated in Sec. III B, and the approach to the product measure is analyzed in Sec. III C. Section IV is devoted to algebraically growing robber functions ($\gamma > 0$). The mean-field theory is first developed for $\gamma = 1$ and then compared to simulations (Sec. IV A). Section IV B examines the case $0 < \gamma < 1$. Conclusions and open questions are formulated in Sec. V.

## II. THE STOCHASTIC RIPPLE MODEL

### A. Definition and simulation algorithm

In the stochastic model a sand ripple is characterized by its mass $m$. The mass variables are integers such that each ripple consists of $m_i$ elementary mass units and occupies a site $i$ on a one-dimensional lattice. The mass is conserved, i.e., $M := \Sigma_i m_i = \text{const}$. The $m_i$ correspond to the length variables $\lambda_i$ used in Eqs. (1) and (2). As mentioned in the Introduction, the mass and the length of ripples are here considered to be indistinguishable. We use different symbols for two reasons. We want to make a clear distinction between (i) the real and integer valued ripple sizes and (ii) between the deterministic and noisy dynamics.

Ripples interact only by exchanging mass with their nearest neighbors at an algebraic mass transfer rate $\Gamma(m) = \Gamma_0 m^{\gamma}$. Since the constant $\Gamma_0$ affects only the time scale it will be set equal to unity from now on. If ripples obtain mass only from one of their neighbors the mass transfer is called (totally) asymmetric. If the mass comes from both neighbors we call the dynamics symmetric. The removal of ripples is done such that lattice sites containing no mass are eliminated from the system.

In the simulations three different initial conditions are used. As random initial conditions we denote the case in which the probability to have a ripple of size $m$ is given by the geometric distribution $(1-q)q^{m-1}$, with $0 < q < 1$. The probability $q$ is related to the mean ripple size as $\langle m \rangle = (1-q)^{-1}$. A distribution $m_i = \langle m \rangle \forall i$ is referred to as monodisperse. The third possibility is a Poisson distribution.

In the dynamical evolution a ripple is first selected randomly and time is incremented by $N(t)^{-1}\Gamma_{\max}^{-1}$, where $N(t)$ is the number of ripples and $\Gamma_{\max}$ is the maximum of all the rates of the ripples in the system at time $t$. Denote the mass of the selected ripple by $m$. If $x < \Gamma(m)/\Gamma_{\max}$, where $x$ is a uniformly distributed random number in the interval $[0,1]$, the ripple gets a unit mass from its nearest neighbor. Otherwise a new ripple is selected and the process is repeated. For

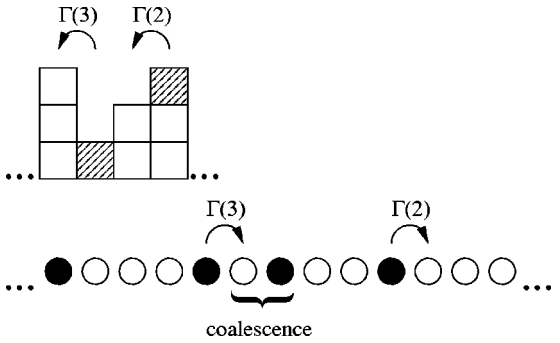


FIG. 2. Mapping between the asymmetric worm model and the exclusion process with coalescence.

symmetric dynamics the neighbor is selected randomly whereas in the asymmetric case it is always the right one.

### B. Relation to other models

In the case of asymmetric dynamics and for $\gamma=-1$ our model reduces to the worm model originally introduced to describe the coarsening of wind ripples [5]. Apart from the extinction step, the sand ripple model is also similar to a zero-range process [6–8]. Both models are defined in terms of conserved, integer mass variables $m_i$ which interact through the exchange of unit masses between nearest neighbor sites of a lattice. The key difference is that in a zero-range process the mass transfer rate is a function of the mass at the site of *departure*, while in the sand ripple model it depends on the mass at the *target* site. This reverses the sign of the right hand sides of Eqs. (1) and (2), and hence the stability properties of the model. The coarsening behavior in zero-range processes with a nonmonotonic robber function is relevant to clustering in granular gases [9].

The occurrence of irreversible extinction events in our model is reminiscent of certain urn models that have been proposed in the context of glassy dynamics [10]. In these models $M$ particles are distributed among $N$ boxes with $m_i$ particles in the $i$th box. In contrast to the ripple model, the urn models have no spatial structure, i.e., mass transfer is possible between any pair of boxes. In the standard dynamical scheme one of the balls is chosen at random and a move to another box is attempted [10]. In our setting this corresponds to a mass transfer rate $\Gamma(m_i)\sim m_i$, where $i$ is the site of *departure*; in this respect the urn models are related to zero-range processes. The extinction corresponds to dynamical rules, where boxes are not refilled once they have become empty. This is the case, for example, in the backgammon model [11] at zero temperature.

The sand ripple model can also be mapped to an exclusion process [7,12,13] along the lines of [14]. The mapping can be done in two ways which differ in how the disappearance of ripples is taken into account. The first alternative is schematically presented in Fig. 2. One constructs a new lattice with $L(t)=M+N(t)$ sites. The mass variables $m_i$ of the ripples turn to $m_i$ consecutive holes separated by particles on sites $i+\Sigma_{k=1}^{i}m_k$ $[i=1,\ldots,N(t)]$. Moving one mass unit from one ripple to its neighbor corresponds to a hop of a particle, and the loss of a ripple becomes a coalescence of particles at contact, which changes the length $L(t)$ of the system.

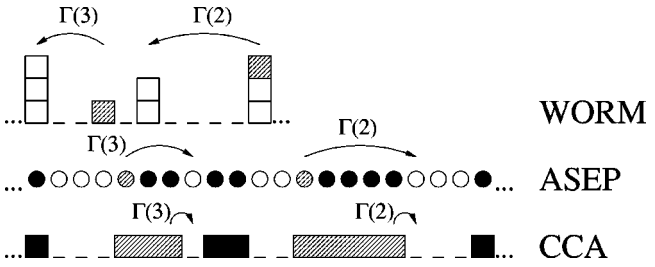


FIG. 3. Mapping between the worm model, the asymmetric exclusion process (ASEP), and the cluster-cluster aggregation (CCA).

For negative (positive) $\gamma$ there is a repulsive (attractive) interaction between the particles. For the marginal case of mass independent transfer rates ($\gamma=0$) the interaction vanishes and the exclusion process reduces to coalescing random walkers, which can be solved exactly [15]. The most relevant results for our case are (i) the average ripple mass grows asymptotically as $\langle m\rangle(t)\sim\sqrt{t}$ and (ii) the ripple size distribution (the probability of finding a ripple of mass $m$ at time $t$) can be written in a scaling form as $p(m;t)=m^{-1}G(m/\langle m\rangle)$, where the scaling function $G(x)=\frac{1}{2}\pi x^2 e^{-\pi x^2/4}$.

A length conserving mapping is obtained by considering the model with ripple extinction but without the removal of empty lattice sites. To avoid creation of new ripples mass is transferred over these sites. In the exclusion process this corresponds to a hop of a particle over all the particles in the same cluster, which can be considered as moving a cluster of particles as a whole (see Fig. 3). In this way our model further maps to a cluster-cluster aggregation process where each cluster moves with a rate that depends on the distance to its neighbor(s). One-dimensional cluster-cluster aggregation models generally obey universal dynamical scaling (see [16] and references therein), which will be seen to be the case also for the sand ripple model.

## III. NOISE-INDUCED COARSENING ($\gamma<0$)

It is known from the mean-field analysis of [5] that for $\gamma=-1$ the average ripple size grows as $\langle m\rangle(t)\approx\ln(t+e^{\langle m\rangle(0)})$. Intuitively, the slow growth follows from the fact that, for $\gamma<0$, the ripples near extinction are those with the highest incoming mass rates. Therefore the disappearance of a ripple involves a rare fluctuation; within the approach of [5], the mass of a ripple evolving in a background of mean mass $\langle m\rangle(t)$ performs a random walk that is biased away from zero.

We base our theoretical analysis on this observation. In what follows, we will assume that at long times, i.e., for large $\langle m\rangle$, the extinction of a ripple is such a rare event that it does not affect the ripple size distribution. Neglecting extinctions, we show that the steady state distribution is given by a product measure. After validating the quasistatic approximation by simulations, we use it to show that to leading order in $t$ the average ripple mass grows as $\langle m\rangle\sim-\gamma^{-1}\ln(t)$. Finally we consider the approach to the product measure by studying nearest neighbor correlations.

### A. Mass distribution

Without extinctions the ripple size distribution can be solved exactly. This is due to the short range of interactions between ripples: The mass transfer rate depends only on the mass at the target site. As was noted above in Sec. II B, this is similar to the zero-range process, where the rate depends only on the site of departure. The most important characteristic of a zero-range process is that its steady state is described by a product measure [8]. This was shown to generalize to processes where the transition rate is a product of functions of the occupation numbers at the site of departure and the target site [17]. As our model is a special case of this class of models, the results of [17] apply here as well. For completeness we give a brief derivation.

The product measure property implies that the stationary probability distribution $P(\{m_i\})$ of finding the system in configuration $\{m_1, m_2, \ldots, m_N\}$ factorizes as

$$P(\{m_i\}) = \prod_i p(m_i), \tag{3}$$

where $p(m_i)$ is the probability of finding mass $m_i$ at site $i$. In the steady state there are no correlations between the ripple sizes. Starting from the master equation for $P(\{m_i\})$ and using the product measure (3), one obtains for the asymmetric case (the calculation is not presented here since up to index changes it is identical to that presented in [8])

$$p(m_i)p(m_{i+1})\Gamma(m_i) = p(m_i+1)p(m_{i+1}-1)\Gamma(m_{i+1}-1). \tag{4}$$

The condition (4), known as pairwise balance [18], generalizes the detailed balance condition familiar from equilibrium statistical mechanics. It has a simple interpretation. The left hand side of Eq. (4) represents the mass transfer to the site $i$, which has to be balanced by a transfer out of this site (the right hand side) in order to be in the steady state. The first two terms give the probability to find a mass $m_i$ at site $i$ with a right neighbor with mass $m_{i+1}$ and the last term describes the rate at which the site $i$ gains mass from its neighbor. We emphasize that, provided a solution to Eq. (4) can be found, this proves that the product measure (3) is an *exact* stationary solution of the master equation; on the basis of general arguments, this solution is then also expected to be unique.

Proceeding similarly for the symmetric dynamics gives (transitions $\{\ldots, m_{i-1}, m_i, m_{i+1}, \ldots\} \to \{\ldots, m_{i-1}, m_i+1, m_{i+1}-1, \ldots\}$ and $\{\ldots, m_{i-1}-1, m_i+1, m_{i+1}, \ldots\} \to \{\ldots, m_{i-1}, m_i, m_{i+1}, \ldots\}$)

$$p(m_{i-1})p(m_i)p(m_{i+1})\Gamma(m_i) = p(m_{i-1}-1)p(m_i+1)p(m_{i+1})\Gamma(m_{i-1}-1). \tag{5}$$

Since $p(m_{i+1})$ cancels out we end up with Eq. (4). Therefore the steady state distribution is independent of the asymmetry of the dynamics.

Equation (4) can be recast as

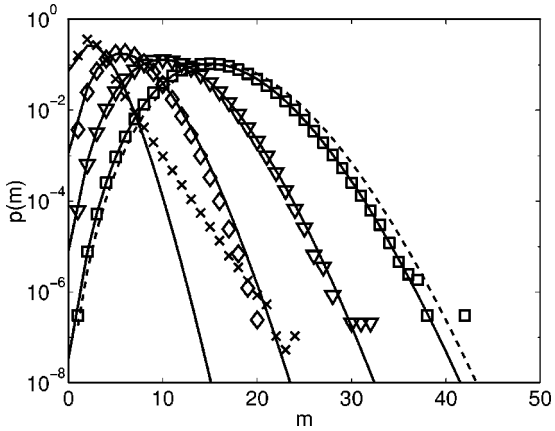


FIG. 4. The ripple size distributions obtained from simulations for $\gamma=-1$ at $t=4$ ($\times$), 256 ($\diamond$), 16 384 ($\nabla$), and 209 7152 ($\square$) together with the analytical result (solid lines) [Eqs. (A2) and (A3)]. The initial distribution at $t=0$ is a random one and simulations are averaged over 2000 runs for a system of size $M=50\,000$. The dashed line shows the asymptotic solution given by Eq. (8) for $t=2\,097\,152$.

$$\alpha^{-1} := \frac{p(m_i)\Gamma(m_i)}{p(m_i+1)} = \frac{p(m_{i+1}-1)\Gamma(m_{i+1}-1)}{p(m_{i+1})}, \tag{6}$$

where $\alpha$ must be a constant. Denoting $p(0)=p_0$ and recursively iterating Eq. (6), we obtain

$$p(m) = p_0\alpha^m \prod_{i=1}^{m-1} \Gamma(i) = p_0\alpha^m[(m-1)!]^\gamma, \tag{7}$$

where the product for $m=1$ is defined to give unity and the last form follows from the definition $\Gamma(m)=m^\gamma$.

The unknown constants $p_0$ and $\alpha$ can be determined by the normalization $\Sigma_{m=0}^{\infty} p(m)=1$ and the expectation value $\langle m\rangle := \Sigma_{m=0}^{\infty} m p(m)$. Explicit results for $\gamma=-1$ and $-2$ can be found in the Appendix A; for $\gamma=-1$, Eq. (7) is a (shifted) Poisson distribution. In general, the distribution for $\langle m\rangle \gg 1$ can be written as

$$p(m) = C_2(\gamma) e^{\gamma\langle m\rangle} \langle m\rangle^{-\gamma m-(1-\gamma)/2}[(m-1)!]^\gamma, \tag{8}$$

where the explicit form of $C_2(\gamma)$ is not important for our purposes. Using the form given in Eq. (8), it is easy to show that the width $\sigma := \sqrt{\langle m^2\rangle - \langle m\rangle^2}$ of the distribution behaves as $\sigma \sim \sqrt{\langle m\rangle}$ independent of $\gamma$.

The calculated distributions are compared to numerics in Figs. 4 and 5. The average ripple mass is not a constant as the simulations include also ripple extinctions. The excellent agreement at long times shows that indeed these become so rare that between subsequent extinctions the system has time to equilibrate to the steady state. Note that all initial distributions converge to the universal distribution $p(m;t)$ given by Eq. (8), where the time dependence enters only through the mean ripple mass $\langle m\rangle(t)$.

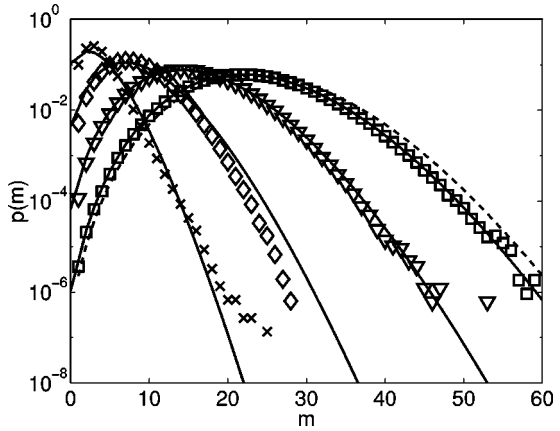


FIG. 5. The ripple size distributions obtained from simulations for $\gamma=-0.5$ at $t=4$ ($\times$),128 ($\diamond$),4096 ($\nabla$), and 131 072 ($\square$) together with the analytical result (solid lines) [Eq. (7)]. The initial distribution at $t=0$ is a random one and simulations are averaged over 500 runs for a system of size $M=50\,000$. The dashed line shows the asymptotic solution given by Eq. (8) for $t=131\,072$.

### B. Coarsening law

Next we proceed to calculate the mean ripple size $\langle m\rangle(t)$ using an approach similar to the analysis of the backgammon model [10]. We assume that, at long times, the probability for a given ripple to vanish is equal to the probability $p(0)$ obtained by extrapolating the steady state probability distribution (8) to $m=0$. The number $N$ of ripples then decays according to $dN/dt\approx -p(0)N$. Since $\langle m\rangle(t)=M/N(t)$ we obtain

$$\frac{d\langle m\rangle(t)}{dt}\approx p(0)\langle m\rangle(t)\sim e^{\gamma\langle m\rangle}\langle m\rangle^{-(1-\gamma)/2}, \tag{9}$$

which to leading order in $t$ gives

$$\langle m\rangle(t)\approx -\gamma^{-1}\ln(t). \tag{10}$$

Simulations with different initial conditions are in accord with Eq. (10) (Fig. 6).

### C. Decay of correlations

The product measure for the ripple size distribution implies that there are no correlations between neighboring ripples. This is true only asymptotically. To study the approach to the product measure distribution we consider the normalized nearest neighbor time correlation function

$$g(t):=\frac{\langle m_i m_{i+1}\rangle-\langle m\rangle^2}{\langle m\rangle^2}. \tag{11}$$

As is clear from Fig. 7, the early time behavior is sensitive to the details of the initial distribution. In this regime it is possible to have positive correlations between neighboring ripples, but at long times there will always be anticorrelations, i.e., $g(t)<0$. The numerically observed correlations seem to be independent of the initial conditions and vanish in a universal manner as

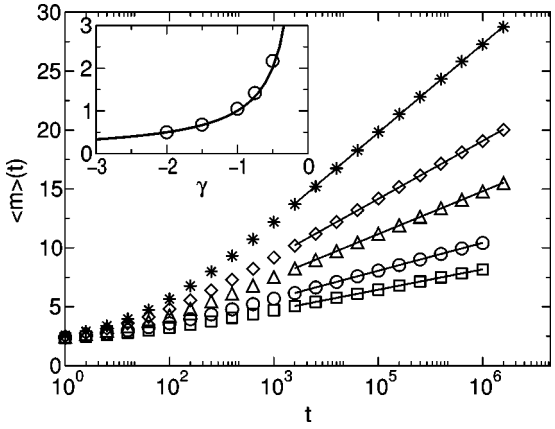


FIG. 6. The growth of the average ripple mass a function of time for $\gamma=-0.5$ (*), $-0.75$ ($\diamond$), $-1$ ($\Delta$), $-1.5$ ($\bigcirc$), and $-2$ ($\square$). The least squares fits are shown by solid lines. The inset compares the fitted prefactors ($\bigcirc$) to the analytic result $-\gamma^{-1}$ (solid line). The system sizes range from 50 000 to 100 000 and averages are taken over at least 50 independent runs.

$$g(t)\sim -t^{-1/2} \tag{12}$$

for both symmetric and asymmetric dynamics.

At first sight one may be tempted to relate the decay of correlations to the extinction events that perturb the product measure. However, as was shown in Sec. III B, the probability of extinction events decays as $p(0)\sim e^{\gamma\langle m\rangle(t)}\sim t^{-1}$, which is much faster than the numerically observed decay law (12). This implies that the power law (12) is associated with the dynamics between extinction events, which can be described using standard hydrodynamic fluctuation theory for a one-dimensional system with a single conserved density.

Let $\phi(x,t)$ denote the coarse grained mass fluctuations in the (quasi-) steady state of mean mass $\langle m\rangle$. The long wavelength behavior of $\phi$ is governed by a Langevin equation of the generic form [19]

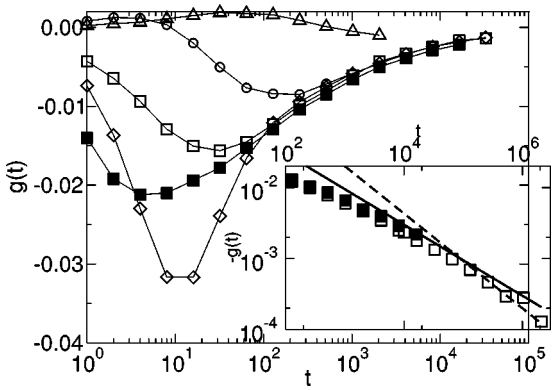


FIG. 7. The nearest neighbor correlation function $g(t)$ for $\gamma=-1$. The initial condition is random [$\langle m\rangle(0)=2,\square;\langle m\rangle(0)=1.2,\blacksquare$], monodisperse [$m(0)=5,\diamond$] or Poisson distributed [$\langle m\rangle(0)=5,\bigcirc;\langle m\rangle(0)=10,\Delta$]. Open (filled) symbols correspond to asymmetric (symmetric) dynamics. The inset shows the decay at late times for the random case. The solid and dashed lines are guides to the eye with slopes $-1/2$ and $-2/3$, respectively.

$$\frac{\partial \phi}{\partial t} = \nu \frac{\partial^2 \phi}{\partial x^2} - \mu \phi \frac{\partial \phi}{\partial x} - \frac{\partial \eta}{\partial x}, \tag{13}$$

where $\eta(x,t)$ is Gaussian white noise with covariance $\langle \eta(x,t)\eta(x',t')\rangle = D\delta(x-x')\delta(t-t')$. For $\mu \neq 0$, Eq. (13) is the noisy Burgers equation [20], which has been widely studied in the context of driven diffusive systems [19] and interface growth [21–23].

The coefficients $\nu, \mu$, and $D$ appearing in the long wavelength description can be related to the microscopic dynamics of the sand ripple model as follows. The nonlinear term on the right hand side of Eq. (13) is generated by the asymmetry, and its coefficient is given by $\mu = j''(\langle m \rangle)$, where $j$ is the steady state mass current. Since in our case $j = \Gamma$, we conclude that $\mu \sim \langle m \rangle^{\gamma-2}$. In the symmetric case $\mu = 0$ and the diffusion coefficient $\nu$ is proportional to $\Gamma' \sim \langle m \rangle^{\gamma-1}$ [this can be seen by expanding Eq. (1) around the homogeneous state]. Finally, owing to a fluctuation-dissipation theorem [20], the equal time correlations of Eq. (13) are Gaussian with covariance $\langle \phi(x)\phi(x')\rangle \sim (D/\nu)\delta(x-x')$ independent of $\mu$. As we have shown above in Sec. III A, in the ripple model the variance of the mass fluctuations is always of order $\langle m \rangle$, hence $D/\nu \sim \langle m \rangle$.

We want to use Eq. (13) to describe the approach to the steady state, starting from some initial condition (e.g., the monodisperse state $\phi \equiv 0$) specified at $t = 0$. The analysis of Eq. (13) shows that at long times, and for $x \neq x'$, the pair correlation function takes the scaling form [22,23]

$$\langle \phi(x,t)\phi(x',t)\rangle = \frac{D}{\nu}\frac{1}{\xi(t)}\mathcal{G}(\xi(t)^{-1}|x-x'|). \tag{14}$$

Here $\mathcal{G}$ is a scaling function and $\xi(t)$ denotes the dynamic correlation length. The prefactor of the scaling function on the right hand side of Eq. (14) is fixed by the requirements that (i) the steady state density fluctuations are proportional to $D/\nu$ and (ii) the integral over the pair correlation function is constant due to mass conservation. The correlation length grows diffusively as $\xi(t) \sim (\nu t)^{1/2}$ for $\mu = 0$ and superdiffusively as $\xi(t) \sim [(D/\nu)^{1/2}\mu t]^{2/3}$ for $\mu \neq 0$.

Keeping $|x-x'|$ fixed and taking $t \to \infty$, we see that the pair correlations (14) decay as $(D/\nu)\mathcal{G}(0)\xi(t)^{-1}$. Expressing $\nu$ and $D/\nu$ in terms of the mean ripple mass, we conclude that in the symmetric case ($\mu = 0$) the normalized correlation function (11) should decay as

$$g(t) \sim \frac{\langle m \rangle^{-(1+\gamma)/2}}{t^{1/2}} \sim \frac{(\ln t)^{-(1+\gamma)/2}}{t^{1/2}}. \tag{15}$$

For $\gamma = -1$ the logarithmic factor disappears and Eq. (15) becomes a pure power law with exponent $-1/2$, in accordance with the simulation results shown in Fig. 7. Moreover, the explicit calculation for the diffusive case shows that the scaling function $\mathcal{G}$ in Eq. (14) is negative, hence $g(t) < 0$ as is observed numerically.

In the asymmetric case the fluctuation theory predicts an asymptotic decay as $g(t) \sim 1/\xi(t) \sim t^{-2/3}$, with logarithmic corrections due to the growth of $\langle m \rangle(t)$. However, this behavior is expected to set in only beyond a crossover time scale $t_\times \sim \nu^5/(D^2\mu^4)$ [23], which for the ripple model takes the form $t_\times \sim \langle m \rangle^{3-\gamma} \sim (\ln t)^{3-\gamma}$. For the case $\gamma = -1$ considered in Fig. 7, this implies that superdiffusive behavior can be expected only for times such that $t/(\ln t)^4 \gg 1$. The left hand side of this inequality becomes equal to unity for $t \approx 5500$ and reaches the value 10 only for $t \approx 235\,000$. The slight deviation of the simulation data from the $t^{-1/2}$ behavior seen after $t = 10^5$ may indicate the beginning of the crossover.

## IV. UNSTABLE COARSENING ($\gamma > 0$)

For $\gamma > 0$ the homogeneous state is linearly unstable because the largest ripples are those with the highest growth rate. Ripple extinction is then no longer a rare event, and the product measure solution derived in Sec. III A becomes invalid. On the other hand, it is plausible (and will be confirmed by simulations, see below) that the linear instability supersedes the noise in the time evolution, so that the deterministic equations (1) and (2) and the stochastic ripple model show the same behavior.

In what follows, we first develop a mean-field theory for the deterministic model in the simplest case of a linear robber function ($\gamma = 1$). Simulations show that the mean-field theory is not quantitatively correct, presumably due to the neglect of spatial fluctuations. In the nonlinear regime $0 < \gamma < 1$ we use scaling analysis to derive the coarsening law.

### A. Mean-field analysis for $\gamma = 1$

We start our analysis from the deterministic equations (1) and (2). For $\gamma = 1$ these become linear but the system is still nontrivial due to the ripple extinction. As the system is deterministic, the only randomness lies in the initial condition. We denote the initial ripple size distribution by $P_0(\lambda_0)$ and its average by $\overline{\lambda_0}$.

The mean-field approximation consists of replacing the ripples surrounding an arbitrary ripple of size $\lambda$ by ripples of the average size $\langle \lambda \rangle$, such that the evolution equation becomes

$$\frac{d\lambda}{dt} = \Gamma(\lambda) - \Gamma(\langle \lambda \rangle) = \lambda - \langle \lambda \rangle. \tag{16}$$

On this level there is no difference between symmetric and asymmetric mass transfer. The solution of Eq. (16) reads $\lambda(\lambda_0, t) = e^t[\lambda_0 - F(t)]$, where the function

$$F(t) := \int_0^t d\tau e^{-\tau}\langle \lambda \rangle(\tau) \tag{17}$$

has to be calculated self-consistently. Note that at this point we do not explicitly restrict $\lambda(t)$ to be non-negative (this constraint will enter later). Once $F(t)$ is known, the ripple size distribution at time $t$ can be obtained by inverting the solution for $\lambda(\lambda_0)$ and inserting this into the initial distribution, with the result

$$p(\lambda;t) = e^{-t}P_0(e^{-t}\lambda + F(t)). \tag{18}$$

Thus in the mean-field approximation the ripple size distribution preserves its initial shape but gets scaled and shifted.

It is possible to derive a differential equation for the unknown function $F(t)$. The fraction $\rho(t)$ of surviving ripples is equal to the probability that $\lambda(t)>0$,

$$\rho(t)=\int_0^\infty d\lambda p(\lambda;t)=\int_{F(t)}^\infty dx P_0(x)=:P_0^c(F(t)), \quad (19)$$

where the last equation defines the cumulative distribution $P_0^c$. The average ripple size is given by $\langle\lambda\rangle(t)=\overline{\lambda_0}/\rho(t)$. Inserting this into the definition of $F(t)$ and differentiating once gives

$$\frac{dF(t)}{dt}=\frac{e^{-t}\overline{\lambda_0}}{P_0^c(F(t))}. \quad (20)$$

Hence the problem reduces to solving the differential equation (20) for a given initial distribution $P_0(\lambda)$.

For example, for an exponential initial distribution $P_0(\lambda_0)=\overline{\lambda_0}^{-1}e^{-\lambda_0/\overline{\lambda_0}}$, we find $F(t)=\overline{\lambda_0}t$ and $\langle\lambda\rangle(t)=\overline{\lambda_0}e^t$, whereas for a flat distribution

$$P_0(\lambda_0)=\begin{cases}(2\overline{\lambda_0})^{-1}, & \lambda_0\leqslant 2\overline{\lambda_0},\\ 0, & \text{otherwise},\end{cases} \quad (21)$$

the solution is given by $F(t)=2\overline{\lambda_0}(1-e^{-t/2})$ and $\langle\lambda\rangle(t)=\overline{\lambda_0}e^{t/2}$. As the rate of exponential growth is different in these two cases, we conclude that the coarsening behavior of the mean-field model (16) is nonuniversal.

In general, the exponential growth rate of the mean ripple size is governed by the extremal statistics of the initial distribution $P_0$. If the initial ripple sizes are bounded by a maximal size $\lambda_{\max}$, and $P_0(\lambda_0)\sim(\lambda_{\max}-\lambda_0)^a$ for $\lambda_0\to\lambda_{\max}$, then the analysis of Eq. (20) shows that $t^{-1}\ln\langle\lambda\rangle(t)\to(a+1)/(a+2)$, while for fat initial distributions with a power law tail, $P_0(\lambda_0)\sim\lambda_0^{-(b+1)}$, we find $t^{-1}\ln\langle\lambda\rangle(t)\to b/(b-1)$.

To compare the predictions of the mean-field theory to simulations we prefer to show the cumulative distribution

$$I(\lambda;t):=\int_\lambda^\infty dx p(x;t)=:f\left(\frac{\lambda}{\langle\lambda\rangle(t)}\right), \quad (22)$$

where the last equation defines the scaling function $f(x)$. A similar definition applies to $p(m;t)$ with the integral replaced by a sum. In the case of an exponential distribution $p(\lambda;t)$ also the function $f(x)$ is exponential whereas for a flat $p(\lambda;t)$ it is linear.

We solved the deterministic equations (1) and (16) using the fourth-order Runge-Kutta method [24]. As a check of the algorithm, we reproduced the solution (18) of the mean-field equations. For the full noiseless system (1) the exponential initial distribution remains unchanged [Fig. 8(a); dashed lines] but also a flat initial distribution presumably approaches the exponential one [Fig. 8(b); dashed lines]. This is in conflict with the mean-field prediction. In both cases the average ripple size grows as $\langle m\rangle(t)\sim e^t$.

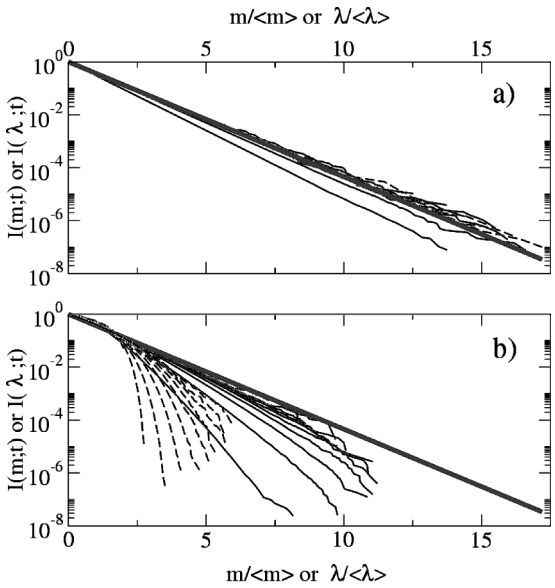


FIG. 8. The complements of the cumulative ripple size distribution for $\gamma=1$. (a) The distributions for random (exponential) initial distribution with noisy (deterministic) dynamics are denoted by solid (dashed) lines. (b) The distributions for monodisperse (flat) initial distribution with noisy (deterministic) dynamics are denoted by solid (dashed) lines. The curves are shown at times $t=1,\ldots,9$ and the thick solid lines in both figures represent the function $e^{-m/\langle m\rangle}$.

Similarly, in the discrete, noisy ripple model the random initial distribution quickly converges towards an exponential scaling function [Fig. 8(a); solid lines]. The monodisperse initial condition spreads out and approaches the same form [Fig. 8(b); solid lines]. Again, the mean ripple size grows as $\langle m\rangle(t)\sim e^t$ for both initial distributions.

Since the deterministic model behaves in a similar manner as the noisy one, we conclude that, in contrast to the case $\gamma<0$, the noise is irrelevant. The discrepancy between the mean-field theory and the full deterministic system suggests that the spatial fluctuations are important, as is often the case for low-dimensional systems. In particular, the numerical results indicate that, in contrast to the mean-field prediction, the behavior of the full system is universal with respect to the initial ripple size distribution. This universality is produced also by another type of mean-field theory [25,26], which is more appropriate for the analysis of high-dimensional systems.

### B. Coarsening law for $0<\gamma<1$

As the mean-field equation is not readily solvable for $\gamma\neq1$ and probably would not describe the problem correctly anyway, here we present a simple scaling argument for the growth of the mean ripple size in the regime $0<\gamma<1$. We start from the observation that in the linearly unstable case $[\Gamma'(\lambda)>0]$, predominantly every second ripple grows and every second one shrinks [4]. Therefore we may consider a simplified system consisting of two ripples of initial sizes $\lambda_1^0>\lambda_2^0$. We calculate the time $t^*$ at which the average size

has doubled. It is given by the conditions $\lambda_1(t^*)=\lambda_1^0+\lambda_2^0$ and $\lambda_2(t^*)=0$. Since the mass is conserved we have $\overline{\lambda} := \lambda_1(t)+\lambda_2(t)=\text{const}$.

Applying Eq. (1) gives

$$\dot{\lambda}_1=\lambda_1^\gamma-\lambda_2^\gamma,$$

$$\dot{\lambda}_2=\lambda_2^\gamma-\lambda_1^\gamma, \tag{23}$$

where the dot denotes derivative with respect to time. The solution is implicitly given by $\lambda_2(t)=\overline{\lambda}-\lambda_1(t)$ and

$$t=\int_{\lambda_1^0}^{\lambda_1(t)}\frac{dx}{x^\gamma-(\overline{\lambda}-x)^\gamma}, \tag{24}$$

which together with the definition of $t^*$ implies the homogeneity relation

$$t^*(a\lambda_1^0,a\overline{\lambda})=a^{1-\gamma}t^*(\lambda_1^0,\overline{\lambda}). \tag{25}$$

Assuming that the evolving ripple size distribution is governed by a single size scale, it follows that the doubling time depends on the mean ripple size as $t^*\sim\langle\lambda\rangle^{1-\gamma}$. The inverse of the doubling time is the growth rate of $\langle\lambda\rangle$. Hence we may write

$$\frac{d\langle\lambda\rangle(t)}{dt}\sim\frac{1}{t^*}\langle\lambda\rangle(t), \tag{26}$$

which yields $\langle\lambda\rangle(t)\sim t^z$ with $z=1/(1-\gamma)$. This is confirmed by simulations, which give $z=1.32\pm0.02$ and $1.98\pm0.03$ for $\gamma=0.25$ and 0.50, respectively. We also numerically checked the universal scaling behavior of the ripple size distribution for $0<\gamma<1$, but in this region the scaling function is more complicated than a simple exponential.

## V. CONCLUSIONS

In this paper we have studied a one-dimensional model for sand ripple evolution, where mass is transferred between neighboring sites with algebraic rates, and sites containing no mass are removed from the system (ripple extinction). As the rates depend only on the site to which the mass is transferred, the system is similar to a zero-range process. Thus the steady state in the absence of ripple extinction is characterized by a product measure. Asymptotically this continues to hold for algebraically decaying mass transfer rates ($\gamma<0$), since the extinctions are exponentially rare at late times. As a consequence the average ripple size grows to leading order logarithmically slowly with the prefactor $-1/\gamma$.

For $\gamma<0$ the approach to the steady state product measure is algebraic. The correlations between masses of neighboring ripples decay universally, i.e., independent of the initial distribution, as $t^{-1/2}$ and $t^{-2/3}$ for symmetric and asymmetric mass transfer, respectively. In the asymmetric case the asymptotic regime is preceded by a long crossover, where $t^{-1/2}$ decay is observed.

For algebraically growing robber functions ($\gamma>0$) the coarsening is driven by the linear instability of the homogeneous state. Ripple extinctions become frequent, and the product measure is no longer relevant. The average ripple size grows algebraically as $t^{1/(1-\gamma)}$ for $0<\gamma<1$. The behavior at $\gamma=0$ is discontinuous since $\langle m\rangle(t)\sim t^{1/2}$ for $\gamma=0$, which follows from the mapping to coalescing random walkers. For $\gamma=1$, $\langle m\rangle(t)\sim e^t$ and the scaling function of the ripple size distribution appears to be a simple exponential. The dynamical noise, which is necessary to have coarsening for $\gamma\leqslant0$, is irrelevant for $\gamma>0$. The mean-field theory developed for $\gamma=1$ reproduces the exponential growth of the mean ripple size, but is insufficient to describe the universality of the growth law and the ripple size distribution which is observed numerically.

It is interesting to compare the results to the behavior in one-dimensional cluster-cluster aggregation. Recall that the model treated here can be mapped to cluster-cluster aggregation with hopping rates of clusters depending algebraically on the distance between them (Sec. II B). When the hopping rates depend as $\Gamma(m)\sim m^\gamma$ on the *masses* of clusters, the growth of the average cluster size is algebraic with $\langle m\rangle(t)\sim t^{1/(2-\gamma)}$ for all $\gamma<2$ [16]. Thus the behavior for nonnegative values of $\gamma$ is rather similar in the two models, but for $\gamma<0$ one finds a drastic difference due to the repulsive interaction between clusters in the ripple model.

We conclude by adducing some open problems for future studies. One of the most interesting issues is to understand the coarsening and the final ripple size selection in the case of a nonmonotonic robber function. This has direct applications in the coarsening of vortex ripples, where the robber function has recently been measured [2]. Initially these systems are in the unstable regime, where the transfer function is monotonically increasing. As we have seen in the present paper, even this is a harder problem than the case where the dominant contribution to coarsening comes from the dynamical fluctuations. For nonmonotonic robber functions one needs an understanding of both coarsening mechanisms. Therefore the starting point into this direction would be to better understand the $\gamma>0$ case.

## ACKNOWLEDGMENTS

E.K.O.H. thanks M. J. Alava for valuable discussions and a critical reading of a preliminary version of the manuscript. He is also indebted to the kind hospitality of the University of Essen where the main part of this research was performed. J.K. is grateful to K. H. Andersen for introducing him to the problem, and to M. R. Evans for mentioning the backgammon model. Financial support by Vilho, Yrjö, and Kalle Väisälä Foundation, DFG within SFB 237, and the Academy of Finland's Center of Excellence program are gratefully acknowledged.

## APPENDIX: CALCULATION OF MASS DISTRIBUTIONS FOR $\gamma=-1$ AND $-2$

Here we calculate the explicit form of the mass distribution

$$p(m)=p_0\alpha^m\prod_{i=1}^{m-1}\Gamma(i)=p_0\alpha^m[(m-1)!]^\gamma, \qquad \text{(A1)}$$

for $\Gamma(m)=m^\gamma$ in the cases $\gamma=-1$ and $-2$. For $m=1$ the product in Eq. (A1) is defined to be unity, and we set $(-1)!=1$. The normalization condition $\Sigma_{m=0}^{\infty}p(m)=1$ gives

$$p(m)=\begin{cases}(1+\alpha e^{\alpha})^{-1}\alpha^m/(m-1)! & \text{for } \gamma=-1\\ I_0^{-1}(2\sqrt{\alpha})\alpha^{m-1}/[(m-1)!]^2 & \text{for } \gamma=-2,\end{cases} \qquad \text{(A2)}$$

where $I_n(x)$ is the modified Bessel function of the first kind. The parameter $\alpha$ is related to the expectation value $\langle m\rangle=\Sigma_{m=0}^{\infty}mp(m)$ by

$$\langle m\rangle=\begin{cases}\alpha(\alpha+1)e^{\alpha}/(1+\alpha e^{\alpha}) & \text{for } \gamma=-1\\ 1+\sqrt{\alpha}I_1(2\sqrt{\alpha})/I_0(2\sqrt{\alpha}) & \text{for } \gamma=-2.\end{cases} \qquad \text{(A3)}$$

Using the expansion $I_n(x)=e^x/\sqrt{2\pi x}+O(1/x)$ for $\alpha\to\infty$, these formulas simplify to $\langle m\rangle\approx\alpha$ and $\langle m\rangle\approx\sqrt{\alpha}$ for $\gamma=-1$ and $-2$, respectively. Hence for $\langle m\rangle\to\infty$ the distributions become

$$p(m)\approx\begin{cases}e^{-\langle m\rangle}\langle m\rangle^{m-1}/(m-1)! & \text{for } \gamma=-1\\ 2\sqrt{\pi}e^{-2\langle m\rangle}\langle m\rangle^{2m-3/2}/[(m-1)!]^2 & \text{for } \gamma=-2,\end{cases} \qquad \text{(A4)}$$

which are of the general form indicated in Eq. (8).


[1] R.A. Bagnold, *The Physics of Blown Sand and Desert Dunes* (Chapman & Hall, London, 1941).

[2] K.H. Andersen, M. Abel, J. Krug, C. Ellegaard, L.R. Sønder-gaard, and J. Udesen, Phys. Rev. Lett. **88**, 234302 (2002).

[3] K.H. Andersen, M.-L. Chabanol, and M. van Hecke, Phys. Rev. E **63**, 066308 (2001).

[4] J. Krug, Adv. Complex Syst. **4**, 353 (2001).

[5] B.T. Werner and D.T. Gillespie, Phys. Rev. Lett. **71**, 3230 (1993).

[6] F. Spitzer, Adv. Math. **5**, 246 (1970).

[7] H. Spohn, *Large Scale Dynamics of Interacting Particles* (Springer-Verlag, New York, 1991).

[8] M.R. Evans, Braz. J. Phys. **30**, 42 (2000); e-print cond-mat/0007293.

[9] D. van der Meer, K. van der Weele, and D. Lohse, Phys. Rev. E **63**, 061304 (2001).

[10] C. Godrèche and J.M. Luck, J. Phys.: Condens. Matter **14**, 1601 (2002).

[11] F. Ritort, Phys. Rev. Lett. **75**, 1190 (1995).

[12] T.M. Liggett, *Interacting Particle Systems* (Springer-Verlag, New York, 1985).

[13] B. Derrida and M.R. Evans, *Nonequilibrium Statistical Mechanics in One Dimension*, 1st ed. (Cambridge University Press, Cambridge, 1997).

[14] S.N. Majumdar, S. Krishnamurthy, and M. Barma, J. Stat. Phys. **99**, 1 (2000).

[15] D. ben-Avraham, *Nonequilibrium Statistical Mechanics in One Dimension*, 1st ed. (Cambridge University Press, Cambridge, 1997).

[16] E.K.O. Hellén, T.P. Simula, and M.J. Alava, Phys. Rev. E **62**, 4752 (2000).

[17] V. Karimipour and B.H. Seradjeh, Europhys. Lett. **57**, 658 (2002).

[18] G. Schütz, R. Ramaswamy, and M. Barma, J. Phys. A **29**, 837 (1996).

[19] H. van Beijeren, R. Kutner, and H. Spohn, Phys. Rev. Lett. **54**, 2026 (1985).

[20] D. Forster, D. Nelson, and M. Stephen, Phys. Rev. A **16**, 732 (1977).

[21] M. Kardar, G. Parisi, and Y. Zhang, Phys. Rev. Lett. **56**, 889 (1986).

[22] J. Krug and H. Spohn, *Solids Far From Equilibrium*, 1st ed. (Cambridge University Press, Cambridge, 1991).

[23] J. Krug, Adv. Phys. **46**, 139 (1997).

[24] W.H. Press, B.P. Flannery, S.A. Teukolsky, and W.T. Vetterling, *Numerical Recipes* (Cambridge University Press, New York, 1986), Chap. 15.1.

[25] S. Ispolatov, P. Krapivsky, and S. Redner, Eur. Phys. J. B **2**, 267 (1998).

[26] F. Leyvraz and S. Redner, Phys. Rev. Lett. **88**, 068301 (2002).